Latin American Journal of Solids and Structures

www.lajss.org

Numerical analysis of highly deformable elastoplastic beams

Abstract

The objective of the present study is to develop a numerical formulation to predict the behavior of highly deformable elastoplastic thin beams. Following the Euler-Bernoulli bending, the axial and shear effects are neglected, and the nonlinear second-order differential equation regarding the angle of rotation is defined based on the specific moment-curvature relationship. Although the formulation can be used for general materials, three constitutive models are employed: linear-elastic, bilinear elastoplastic, and linear-elastic with Swift isotropic hardening. The resultant boundary value problem is solved by means of the fourth-order Runge-Kutta integration procedure and the one-parameter nonlinear shooting method. The performance of the present formulation is investigated via three numerical problems involving finite bending of slender beams composed of elastoplastic materials. For these problems, numerical solutions regarding rotations, displacements and strains for the loading, unloading and reloading phases are provided. Finally, it is shown that the present methodology can also be used to determine the post-buckling behavior of elastoplastic thin beams.

João Paulo Pascon

Materials Engineering Department, Lorena School of Engineering, University of São Paulo
Polo Urbo-Industrial Gleba AI-6, PO box 116, Zip code 12600-970
Lorena, São Paulo, Brazil

Corresponding author:
jppascon@usp.br

1 INTRODUCTION

Bending of highly deformable materials is a very interesting topic. In this context, several engineering applications can be cited: transmission cables, suspension springs, aerospace vehicle wings, rotor blades, solar collectors, dish antennas and space stations. In general, these structures are flexible, i.e., may present large deflections when loaded. To describe the equilibrium of forces in finite deflections, the geometrically nonlinear analysis is imperative. To circumvent the resultant complexity, numerical methods are usually employed.

For slender (or thin) beams, a reasonable approach is the Euler-Bernoulli hypothesis: plane cross sections remain plane and orthogonal to the deformed axis. Another condition usually imposed is the inextensibility of the beam axis. For plane beams (or two-dimensional bending), the warping is not considered. These three assumptions can be extended to finite deformations. Based on these hypotheses, the axial, torsion and shear effects are neglected and, thus, the bending moment is the dominant internal action. The Euler-Bernoulli bending for finite deflections has been extensively used in the scientific literature, since the work of Bisshopp and Drucker (1945), which have defined the differential equation to be solved involving the exact curvature for large displacements, since the assumptions from elementary beam theory are no longer valid. Based on this differential equation, various works dealing with finite Euler-Bernoulli bending have been performed (see, among many others, Jenkins et al. (1966); Holden (1972); Mattiasson (1981); Lee (2002); Chen (2010); Tari (2013)).

Regarding the material behavior, the deformations (or strains) may be elastic (reversible) or plastic (permanent). Large elastic strains are common in the context of elastomers, and large plastic deformations occur, for instance, in sheet-metal forming processes. Neglecting the shear effects, a uniaxial stress-strain relationship can be used. Even in the finite displacement analysis, the Hooke's law can be used if the elastic strain level is small. For moderate elastic strains, a usual constitutive law is the Ludwick material model (see, for example, Lee (2002); Lewis and Monasa (1981); Monasa and Lewis (1983); Carrillo (2009)). This model has been firstly applied to the finite Euler-Bernoulli bending in the work of Lewis and Monasa (1981). In the elastoplastic regime, there are many uniaxial models that can be used for beams (see, for instance, Hutchinson (1972); Chan et al. (1991); Cimetière and Léger (1996); Durban and Zuckerman (1999)): bilinear, multi-linear, Ramberg-Osgood, linear elastic with hardening etc. An important and very suitable model for sheet-metal forming processes is the Swift isotropic hardening law (Swift, 1947).

In solid mechanics, the bending moment is connected to the normal longitudinal stress, and the bending curvature is associated with the normal longitudinal strain. Combining these relations with the uniaxial material model, a moment-curvature relationship can be defined to analyze plane beams, for example. Obviously, this relationship is modified when the material exceeds the elastic limit and reaches the elastoplastic domain. In the work of Lewis et al. (1987), for instance, a moment-curvature relationship for partially yielded rectangular cross-section is employed.

In the context of finite (or nonlinear) bending, the usual procedure is to set the nonlinear second-order differential equation regarding the angle of rotation defined as a function of the curvilinear coordinate. In order to solve this equation, the two most common numerical techniques are: the use of elliptic integrals (see, for example, the works of Bisshopp and Drucker (1945); Jenkins et al. (1966); Mattiasson (1981); Sinclair (1979)); and the use of numerical integration along the curvilinear coordinate (see, for instance, Holden (1972); Lewis et al. (1987); Rao and Rao (1989)). In order to avoid the use of elliptic integrals, which are quite complicated, the second strategy has been adopted in this paper. Following the works of Holden (1972), Lee (2002), Lewis and Monasa (1981), Monasa and Lewis (1983) and Rao and Rao (1989), the differential second-order equation is expressed as a system of two first-order equations, whose numerical solution is found via the fourth-order Runge-Kutta scheme and the nonlinear one-parameter shooting method. As the angle of rotation is defined, the plane Cartesian coordinates can be found, for example, by means of the trapezoidal integration rule.

A specific and very important related problem is the post-buckling behavior of elastoplastic thin beams. In this context, several works can be cited as, for example, Hutchinson (1972), Cimetière and Léger (1996), Kounadis and Mallis (1987), Léger and Potier-Ferry (1993) and Grognec and Le van (2011). However, very few papers deal with the unloading and reloading phases, which is a topic that can be used, for instance, in the analyses of truss-like structures composed of elastoplastic materials. Moreover, in most of the related papers, the perfectly elastoplastic, bilinear and Ramberg-Osgood elastoplastic models are employed. No Swift isotropic hardening law together with post-buckling behavior has been found along the bibliographic research performed.

The objective of this study is to develop a numerical formulation to predict the behavior of highly deformable thin beams composed of elastoplastic materials, including bilinear and Swift isotropic hardening elastoplastic laws. As said before, this formulation can be implemented in a computer code developed for nonlinear analysis of lattice structures, especially for compressed elastoplastic members. Although the present large-deformation analysis can be performed in a general way by means of the Finite Element Method (FEM), the intention here is to show an alternative simple technique to obtain some numerical solutions for elastoplastic thin beams.

Besides the Introduction, this paper is organized in four sections. The formulation regarding the nonlinear bending is described in section 2. The numerical procedure to solve the nonlinear second-order differential equation is explained in section 3. The validating numerical results, as well as their discussion, are provided in the fourth section. Finally, the main conclusions are given in section 5.

2 BENDING PROBLEM

In this paper, the effects of shearing, axial deformation and warping are neglected, and the extension of the Euler-Bernoulli hypothesis to finite deflections and rotations is used:

$$\frac{1}{\rho} = \frac{\mathrm{d}\theta}{\mathrm{d}s} \tag{1}$$

where $1/\rho$ is the bending curvature; θ is the angle of rotation; and s is the curvilinear coordinate (see Figure 1). Adopting the inextensibility condition of the beam axis, the curvilinear coordinate s varies from 0 to L, where L is initial length of the beam. Therefore, considering a rectangular cross section with width b and height $2c$, the longitudinal normal strain (ε) is null at the centroid and varies along the height, from $-\varepsilon_{\max}$ at the lower edge to $\varepsilon_{\max}$ at the upper edge. According to Figure 1, if the upper edge is elongated, the value of $\varepsilon_{\max}$ is positive and the angle θ decreases. Thus, one can associate the curvature (1) with the maximum value of the strain as follows:

$$\frac{\mathrm{d}\theta}{\mathrm{d}s} = -\frac{\varepsilon_{\max}}{c} \tag{2}$$

From equation (2), to associate the internal bending moment (M) with the curvature ($\mathrm{d}\theta/\mathrm{d}s$), one needs to define the constitutive law (or the stress-strain relation). Three cases are analyzed here: fully linear-elastic cross section; partially yielded cross section with bilinear elastoplastic material; and partially yielded cross section with Swift isotropic hardening model. For the three cases, the
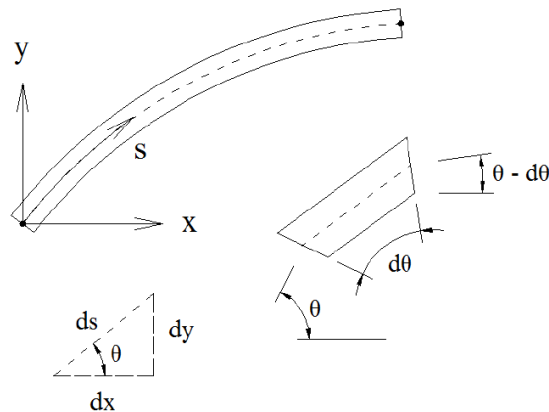
Figure 1: Coordinates and angle of rotation at the current (deformed) configuration. The symbols x and y denote the rectangular coordinates.

moment M depends on the maximum strain ($\varepsilon_{\max}$), which is related to the curvature via equation (2). So, in order to obtain the moment-curvature relationship, one needs to determine the derivative of M regarding s:

$$\frac{\mathrm{d}M}{\mathrm{d}s} = \frac{\mathrm{d}M}{\mathrm{d}\varepsilon_{\max}}\frac{\mathrm{d}\varepsilon_{\max}}{\mathrm{d}s} = \frac{\mathrm{d}M}{\mathrm{d}\varepsilon_{\max}}\left(-c\frac{\mathrm{d}^2\theta}{\mathrm{d}s^2}\right) \Rightarrow \frac{\mathrm{d}^2\theta}{\mathrm{d}s^2} = -\frac{1}{c}\frac{\mathrm{d}M}{\mathrm{d}s}\left(\frac{\mathrm{d}M}{\mathrm{d}\varepsilon_{\max}}\right)^{-1} \tag{3}$$

where $M(\varepsilon_{\max})$ is the specific function that associates the internal bending moment with the maximum normal strain.

For the first case, the uniaxial Hooke's law is employed and, thus, a well-known relation is obtained (see equation (2)):

$$M = \int_A \sigma Y \mathrm{d}A = \int_A (E\varepsilon) Y \mathrm{d}A = \int_A E\frac{\varepsilon_{\max}}{c} Y^2 \mathrm{d}A = \frac{\varepsilon_{\max}}{c} EI_z \Rightarrow \frac{\mathrm{d}^2\theta}{\mathrm{d}s^2} = -\frac{1}{EI_z}\frac{\mathrm{d}M}{\mathrm{d}s} \tag{4}$$

where σ is the longitudinal normal stress; Y is the distance along the height from the centroid (see Figure 1); E is the Young modulus; and I_z is the moment of inertia regarding the z axis, which is normal to the bending plane.

For the second and third cases, as the material exceeds the elastic limit, a central portion of the cross remains in elastic domain, and the extreme lower and upper portions reach the elastoplastic regime (see Figure 2). Considering the bilinear elastoplastic material, the stress-strain relationship is:

$$\sigma = E\varepsilon \text{, for } \varepsilon < \varepsilon_Y \text{ or } |Y| < Y_p \tag{5}$$

$$\sigma = \sigma_Y + E_p(\varepsilon - \varepsilon_Y) \text{, for } \varepsilon > \varepsilon_Y \text{ or } |Y| > Y_p \tag{6}$$

where ε_Y, σ_Y and E_p are, respectively, the yield strain, the yield stress and the plastic modulus, obtained from the uniaxial tension test. Considering (5) and (6), it is possible to show that the function is modified to:
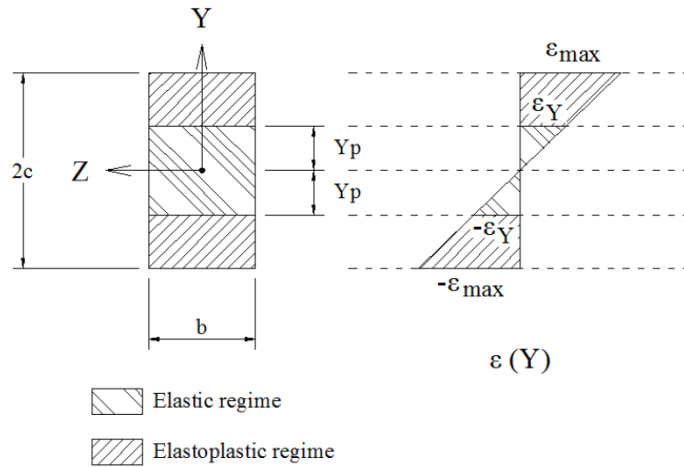
Figure 2: Partially yielded rectangular cross section.

$$M = bc^2 \left\{ \left(E - E_p \right)\varepsilon_Y + \left(\frac{2E_p}{3} \right)\varepsilon_{\max} + \left[\varepsilon_Y{}^2 \left(\frac{2E\varepsilon_Y}{3} + \frac{E_p\varepsilon_Y}{3} - E\varepsilon_Y \right) \right] \varepsilon_{\max}{}^{-2} \right\} \tag{7}$$

Combining this expression with the result in (3):

$$\frac{\mathrm{d}^2\theta}{\mathrm{d}s^2} = -bc\frac{\mathrm{d}M}{\mathrm{d}s} \left\{ \left(\frac{2E_p}{3} \right) - 2\left[\varepsilon_Y{}^2 \left(\frac{2E\varepsilon_Y}{3} + \frac{E_p\varepsilon_Y}{3} - \sigma_Y \right) \right] \varepsilon_{\max}{}^{-3} \right\}^{-1} \tag{8}$$

Finally, for the Swift isotropic hardening model, it is assumed that the elastic strains are small compared with the plastic strains and, thus, all the strain is plastic in the elastoplastic regime:

$$\sigma = E\varepsilon, \text{ for } \varepsilon < \varepsilon_Y \text{ or } \left| Y \right| < Y_p \tag{9}$$

$$\sigma = K\left(\varepsilon_0 + \varepsilon \right)^n, \text{ for } \varepsilon > \varepsilon_Y \text{ or } \left| Y \right| > Y_p \tag{10}$$

where K, ε_0 and n are the Swift coefficients. As in expression (4), the integration of the bending moment due to the stresses (9) and (10) leads to:

$$M = \frac{a_1}{\varepsilon_{\max}{}^2} + \frac{b_1\left(\varepsilon_0 + \varepsilon_{\max} \right)^{n+1}}{\varepsilon_{\max}} + \frac{b_2}{\varepsilon_{\max}{}^2} + \frac{b_3\left(\varepsilon_0 + \varepsilon_{\max} \right)^{n+2}}{\varepsilon_{\max}{}^2} + \frac{b_4}{\varepsilon_{\max}{}^2} \tag{11}$$

$$a_1 = EI_z \frac{\varepsilon_Y{}^3}{c} \tag{12}$$

$$b_1 = \frac{2Kbc^2}{n+1} \tag{13}$$

$$b_2 = -\frac{2Kbc^2}{n+1}\left(\varepsilon_0 + \varepsilon_Y \right)^{n+1}\varepsilon_Y \tag{14}$$

$$b_3 = -\frac{2Kbc^2}{(n+1)(n+2)} \tag{15}$$

$$b_4 = \frac{2Kbc^2}{(n+1)(n+2)}\left(\varepsilon_0 + \varepsilon_Y\right)^{n+2} \tag{16}$$

Therefore, the derivative that appears in (3) is:

$$
\begin{aligned}
\frac{\mathrm{d}M}{\mathrm{d}\varepsilon_{\max}} = &-2\Big[a_1 + b_2 + b_4 + b_3\left(\varepsilon_0 + \varepsilon_{\max}\right)^{n+2}\Big]\varepsilon_{\max}^{-3} + \\
&\Big[b_3\left(n+2\right)\left(\varepsilon_0 + \varepsilon_{\max}\right)^{n+1} - b_1\left(\varepsilon_0 + \varepsilon_{\max}\right)^{n+1}\Big]\varepsilon_{\max}^{-2} + \Big[b_1\left(n+1\right)\left(\varepsilon_0 + \varepsilon_{\max}\right)^{n}\Big]\varepsilon_{\max}^{-1}
\end{aligned}
\tag{17}
$$

3 NUMERICAL PROCEDURE

For a beam with prescribed boundary conditions (loading and rotations), as showed in the last section, one needs to solve a nonlinear second-order differential equation regarding the function $\theta(s)$ (see the result of expression (3)). In general, a beam has a prescribed value at each one of the two ends: a rotation or a bending moment. So, the differential equation together with the two prescribed values is classified as a two-point boundary value problem. The procedure adopted here consists in dividing this equation in a system of two initial value problems (IVPs). To do this, two auxiliary functions are used: $f_1(s) = \theta$ and $f_2(s) = \mathrm{d}\theta/\mathrm{d}s$. With these functions, we write the following system of two IVPs:

$$\frac{\mathrm{d}f_1}{\mathrm{d}s} = f_2, \ \ f_1(0) = \theta_0 \tag{18}$$

$$\frac{\mathrm{d}f_2}{\mathrm{d}s} = -\frac{1}{c}\frac{\mathrm{d}M}{\mathrm{d}s}\left(\frac{\mathrm{d}M}{\mathrm{d}\varepsilon_{\max}}\right)^{-1}, \ \ f_2(0) = \left(\frac{\mathrm{d}\theta}{\mathrm{d}s}\right)_0 \tag{19}$$

where θ_0 and $\left(\mathrm{d}\theta/\mathrm{d}s\right)_0$ are the initial values at the end of the beam in which the origin of s is placed. Even in the case of nonlinear systems, if these values are known, the solution of the system can be found via a numerical procedure. In this study, the beam is split into a finite number of segments and the fourth-order Runge-Kutta method is employed to solve the system of equations (18) and (19). Once determined the values of θ and $\mathrm{d}\theta/\mathrm{d}s$ at the extreme points of each segment, the rectangular coordinates x and y can be obtained via numerical integration. From Figure 1, these coordinates are determined using the trapezoidal rule:

$$\Delta x = x(s + \Delta s) - x(s) = \int_s^{s+\Delta s} \cos\theta \ \mathrm{d}s \approx \frac{\Delta s}{2}\Big[\cos(\theta) + \cos(\theta + \Delta\theta)\Big] \tag{20}$$

$$\Delta y = y(s + \Delta s) - y(s) = \int_s^{s+\Delta s} \sin\theta \ \mathrm{d}s \approx \frac{\Delta s}{2}\Big[\sin(\theta) + \sin(\theta + \Delta\theta)\Big] \tag{21}$$

where the symbol Δ denotes the finite variation of some quantity along the segment. As the equilibrium is described at the final (deformed) configuration, x and y are the final rectangular coordinates.

The problem in applying the Runge-Kutta procedure to the system of equations (18) and (19) is that the initial values θ_0 and $\left(d\theta/ds \right)_0$ are not simultaneously known at one of the two ends of the beam. For example, in a cantilever beam under a free-end shear force, the bending moment at the free end is zero and, hence, $\left(d\theta/ds \right)_0 = 0$. However, the angle of rotation at this point is not prescribed and, thus, the integration of equation (18) from the free end to the clamped edge depends on the unknown value θ_0. To deal with this inconvenient, the shooting method is used. In the case of the above-mentioned cantilever, the sequence of IVPs (18) and (19) are solved in such a way that the solution converges to $\theta = 0$ at the clamped edge. Therefore, the objective is to find the angle of rotation at the free end (θ_0) that corresponds to the null rotation at the clamped edge. As there is only one parameter (θ_0) and the differential equation is nonlinear, the applied method is the one-parameter nonlinear shooting method. Alternatively, if the integration is performed from the clamped edge to the free end, the objective is to determine the initial value $\left(d\theta/ds \right)_0$ that corresponds to $\theta = 0$ at the clamped edge and $d\theta/ds = 0$ at the free end.

During the loading phase, the solution clearly depends on the material regime. The differential equation is modified if the material exceeds the elastic limit (see expressions (3), (4), (8) and (17)). If the beam reaches the elastoplastic regime, the first task is to determine the curvilinear coordinate (s^*) that corresponds to the threshold between the elastic and elastoplastic parts of the beam. This determination is done based on the yield stress limit (σ_Y). In the case of a bending moment increasing along the curvilinear coordinate, if the maximum stress at $s = s_n$ is lower than σ_Y, and the maximum stress at $s = s_n + 1$ is higher than σ_Y, the size of interval $\Delta s = s^* - s_n$ is updated until the integration from s_n provides a maximum stress sufficiently close to σ_Y. As this threshold is obtained, the integration considering the elastoplastic regime is performed from $s = s^*$ to $s = L$.

For the unloading phase, it is assumed that the material response is purely elastic and, thus, equation (4) together with the solution obtained from the end of the loading can be used. To guarantee that the response is purely elastic for the bilinear elastoplastic material, the hardening is assumed to be isotropic and, thus, the stress limit is not changed as occurs in kinematic hardening. Assuming that the applied forces are completely removed, the internal bending moment returns to zero along the entire beam. If $\bar{M}$ is the function that describes the internal moment along the beam length at the last step of the loading phase, then:

$$\overline{M} + \Delta M = 0 \Rightarrow \Delta M = \int_A \Delta\sigma Y \, dA = \frac{\Delta\varepsilon_{\max}}{c} EI_z = -\overline{M} \Rightarrow \Delta\varepsilon_{\max} = -\frac{\overline{M}c}{EI_z} \qquad (22)$$

Of course, along the part of the beam that remained in elastic regime, the strains return to zero, and the permanent (or residual) strain remains even after the complete unloading for the elastoplastic part.

Along the reloading phase, if the material remains in elastic regime, the equation (4) can also be employed. Otherwise, one of the elastoplastic equations (8) or (17) must be solved. However, even in the case of a complete unloading followed by reloading, the curvature $d\theta/ds$ is not zero along the

elastoplastic part of beam. For this part, the integration along the reloading phase, after a complete unloading, is performed as follows:

$$\frac{d^2\theta}{ds^2} = \left[\frac{d^2\theta}{ds^2}\right]_U - \frac{1}{c}\frac{dM}{ds}\left(\frac{dM}{d\varepsilon_{\max}}\right)^{-1} \tag{23}$$

where $\left[d^2\theta\big/ds^2\right]_U$ is the second derivative $d^2\theta\big/ds^2$ corresponding to the complete unloaded configuration. The determination of this derivative can be done noting, from equation (22), that:

$$\left(\frac{d\theta}{ds}\right)_U = \left(\frac{\varepsilon_{\max}}{c}\right)_U = \frac{1}{c}\left(\overline{\varepsilon}_{\max} - \Delta\varepsilon_{\max}\right) = \frac{\overline{d\theta}}{ds} - \frac{\overline{M}}{EI_z} \tag{24}$$

where the subscript U denotes the value at the end of the complete unloading phase; and the top bar corresponds to the value at the end of the loading phase. With the values of $\left(d\theta\big/ds\right)_U$ obtained, the following mid-point rule is employed:

$$\left\{\left[\frac{d^2\theta}{ds^2}\right]_U\right\}_i = \frac{1}{2}\left\{\frac{\left[\left(\frac{d\theta}{ds}\right)_U\right]_i - \left[\left(\frac{d\theta}{ds}\right)_U\right]_{i-1}}{s_i - s_{i-1}} + \frac{\left[\left(\frac{d\theta}{ds}\right)_U\right]_{i+1} - \left[\left(\frac{d\theta}{ds}\right)_U\right]_i}{s_{i+1} - s_i}\right\} \tag{25}$$

For the extreme points (i.e., the free ends), the following expressions are used:

$$\left\{\left[\frac{d^2\theta}{ds^2}\right]_U\right\}_{s=0} = \frac{\left[\left(\frac{d\theta}{ds}\right)_U\right]_1 - \left[\left(\frac{d\theta}{ds}\right)_U\right]_0}{s_1 - s_0} = \frac{\left[\left(\frac{d\theta}{ds}\right)_U\right]_1 - \left[\left(\frac{d\theta}{ds}\right)_U\right]_0}{s_1} \tag{26}$$

$$\left\{\left[\frac{d^2\theta}{ds^2}\right]_U\right\}_{s=L} = \frac{\left[\left(\frac{d\theta}{ds}\right)_U\right]_N - \left[\left(\frac{d\theta}{ds}\right)_U\right]_{N-1}}{s_N - s_{N-1}} = \frac{\left[\left(\frac{d\theta}{ds}\right)_U\right]_N - \left[\left(\frac{d\theta}{ds}\right)_U\right]_{N-1}}{L - s_{N-1}} \tag{27}$$

4   NUMERICAL RESULTS

In order to validate the present methodology, three cases involving bending of highly deformable elastoplastic beams are analyzed. For each situation, the shooting method parameter used is specified, and the numerical solutions regarding rotation, final coordinates and longitudinal normal strain are provided. In all the problems, the load is applied incrementally, i.e., in load steps. The first two tries for the shooting method parameter are very close to the last step, and the subsequent tries are estimated via the one-dimensional secant method:

$$X_i = X_{i-1} - F_{i-1}\left(\frac{X_{i-1} - X_{i-2}}{F_{i-1} - F_{i-2}}\right) \tag{28}$$

where X_i is the corresponding value of the parameter X at the current try I; and F is the residue related to the prescribed value of the parameter X.

4.1 Cantilever beam under free-end force

The first case is one of the most analyzed beam problems (see Figure 3). Although there is internal shear, only the effect of the internal bending moment is considered here. Three materials are employed: linear-elastic, bilinear elastoplastic and linear-elastic with Swift isotropic hardening. The first two are general materials, and the third corresponds to the mild steel DC06, whose coefficients have been extracted from [22]. From figure 3, one can see that the bending moment is $M(s) = Px = P\int_s \cos\theta \, \mathrm{d}s$ and, hence, the boundary value problem in this case is:

$$\frac{\mathrm{d}^2\theta}{\mathrm{d}s^2} = -\frac{P\cos\theta}{c}\left(\frac{\mathrm{d}M}{\mathrm{d}\varepsilon_{\max}}\right)^{-1}, \quad \theta(L) = \frac{\mathrm{d}\theta}{\mathrm{d}s}(0) = 0 \tag{29}$$

The corresponding system of IVPs is:

$$\frac{\mathrm{d}f_1}{\mathrm{d}s} = f_2, \quad f_1(0) = \theta_0 \tag{30}$$

$$\frac{\mathrm{d}f_2}{\mathrm{d}s} = -\frac{P\cos f_1}{c}\left(\frac{\mathrm{d}M}{\mathrm{d}\varepsilon_{\max}}\right)^{-1}, \quad f_2(0) = 0 \tag{31}$$

The cantilever beam is divided into 50 segments, and the residue F (see equation 28) is the value of the angle of rotation at the clamped edge.
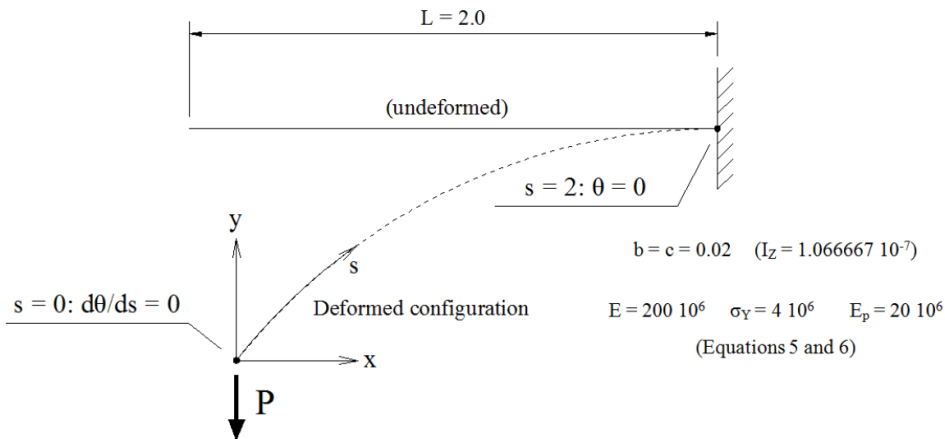
Figure 3: Cantilever beam under free-end force (loading, geometry and material coefficients).

The linear-elastic results are compared to the numerical results of Mattiasson (1981) and Pai and Palazotto (1996). In these references, the second-order nonlinear differential equation regarding the angle of rotation is set, and numerical integration procedures are employed to solve the boundary

value problem. However, the effects of shear and extensibility are taken into account only in the second reference. As these effects are neglected in this study, the present solution is approximately the same as the first reference, and there are small differences between the present and the second reference solution (see Figure 4). If the material remains in elastic regime, there is no reason in analyzing the unloading and reloading phases.

(a)   (b)
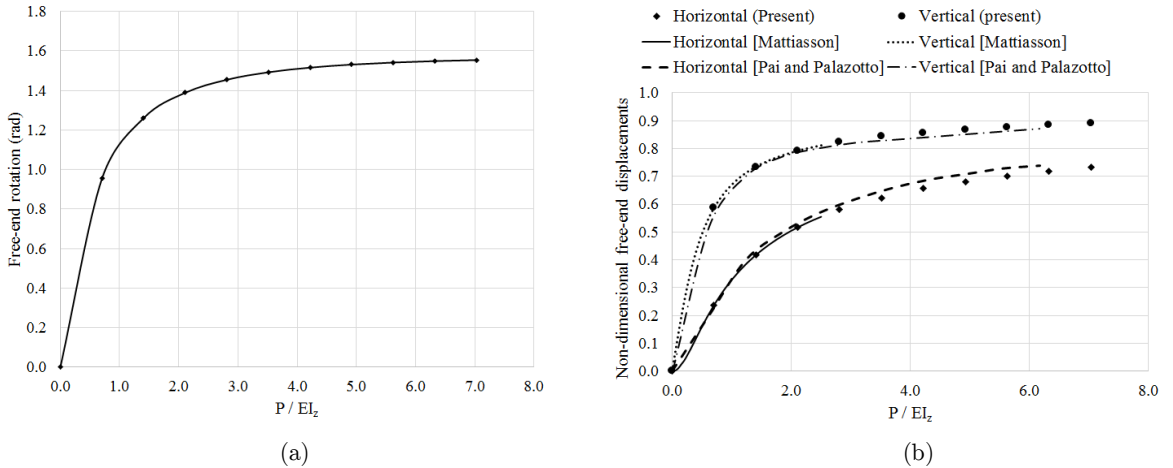
Figure 4: Elastic results for the cantilever of figure 3 under different load levels: (a) angle of rotation; (b) free-end displacements u_x/L and u_y/L.

Once the beam exceeds the elastic limit, the elastoplastic part ($s^* < s < L$) is divided into 50 segments. The numerical results regarding the bilinear elastoplastic material are provided in Figures 5 and 6. At the end of the loading phase, one part of the beam (defined by $0 < s < 1.575$) remains in elastic regime, and the other part ($1.575 < s < 2.0$) is in elastoplastic regime. When the load is completely removed, the first part stays straight as the strain returns to zero. However, the displacements and rotation of the free end do not return to zero due to the plastic (permanent) strains at the second part, which remains curved.
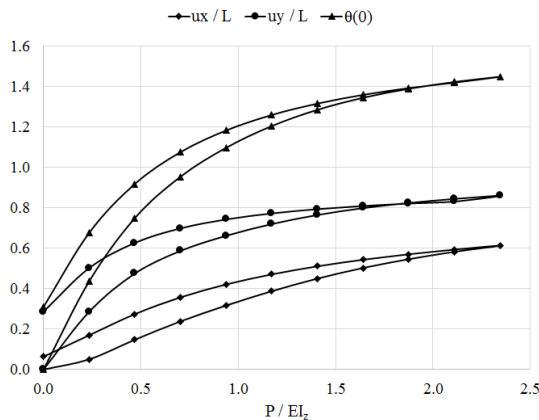
Figure 5: Free-end non-dimensional displacements and angle of rotation for the bilinear elastoplastic cantilever. The symbol "$\theta(0)$" denotes the angle of rotation of the free end.
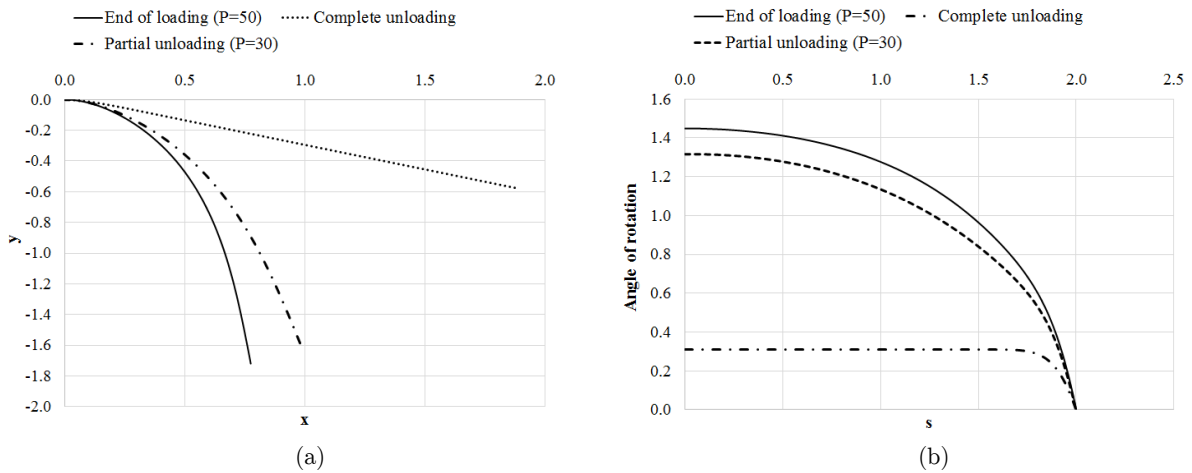
Figure 6: Coordinates from the clamped edge, and angle of rotation along the cantilever beam composed of bilinear elastoplastic material: end of loading ($P = 50$); complete unloading ($P = 0$); and partial unloading ($P = 30$).

The results regarding the third material (linear-elastic with Swift isotropic hardening) are given in Figures 7 and 8. As in the case of the bilinear elastoplastic material, when the load is completely removed, the free-end rotation and displacements do not return to zero, and the elastic part stays straight. The influence of the adopted plastic coefficients on the beam behavior can be seen by comparing Figure 5 to 7, and 6 to 8. One can note that the level of displacements are very close, but the applied force is much smaller for the third material. Besides, the difference between configurations at the end of the loading and the complete unloading is much smaller for the third material. These facts mean that the second material is more rigid and presents higher levels of elastic strain.
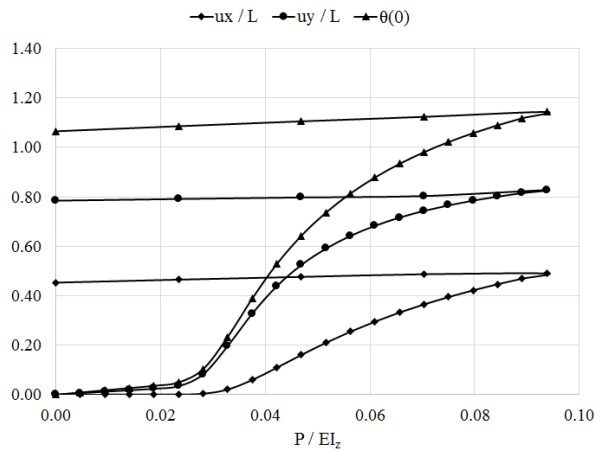
Figure 7: Free-end non-dimensional displacements and angle of rotation for the Swift-case elastoplastic cantilever.

For the three materials, the maximum longitudinal normal strain occurs at the upper edge at the clamp. The corresponding values are provided in Tables 1-3. For the elastic material, there is no plastic strain and, thus, the strain at all the points returns to zero if the load is completely removed.

(a)   (b)
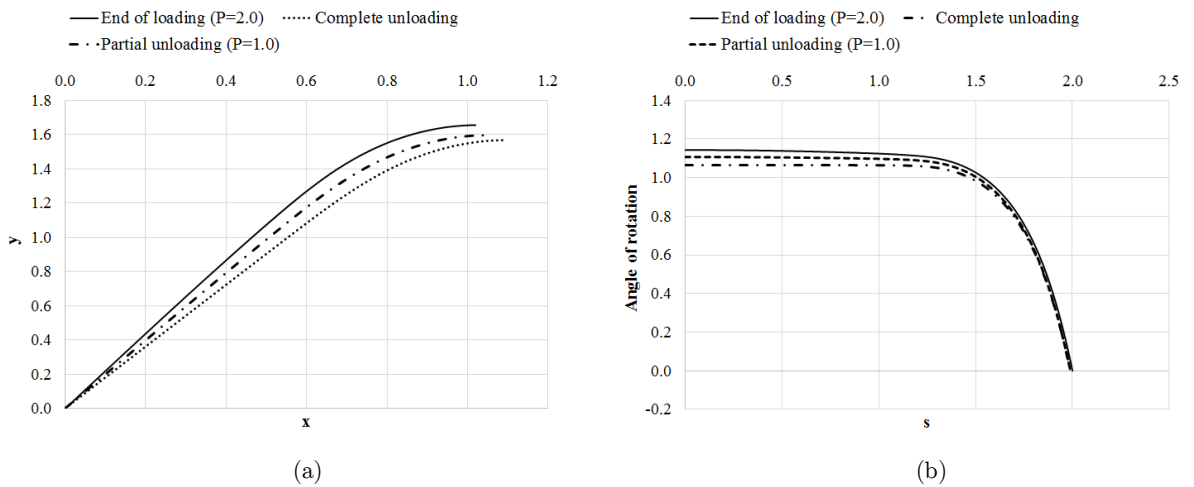
Figure 8: Coordinates from the clamped edge, and angle of rotation along the cantilever beam composed of linear-elastic material with Swift isotropic hardening: end of loading ($P = 2.0$); complete unloading ($P = 0$); and partial unloading ($P = 1.0$).

Phase	End of loading	Complete unloading
Load level	150.0	0.0
$\varepsilon_{\max}$ (%)	7.499	0.000

Table 1: Maximum value of the longitudinal normal strain for the cantilever composed of linear-elastic material.

Phase	End of loading	Complete unloading	Partial unloading
Load level	50.0	0.0	30.0
ε_{max} (%)	9.646	6.020	8.689

Table 2: Maximum value of the longitudinal normal strain for the cantilever composed of bilinear elastoplastic material.

Phase	End of loading	Complete unloading	Partial unloading
Load level	2.0	0.0	1.0
ε_{max} (%)	9.696	9.513	9.380

Table 3: Maximum value of the longitudinal normal strain for the cantilever composed of linear-elastic material with Swift isotropic hardening.

Regarding the two elastoplastic materials, the portion of plastic strain is larger for the third material when compared to the second material. The influence of the material type on the strain levels can be explained by analyzing the graphs of Figure 9. One should remember that, in the case of the present cantilever, the maximum amount of plastic strain corresponds to the value of strain at which the bending moment returns to zero.
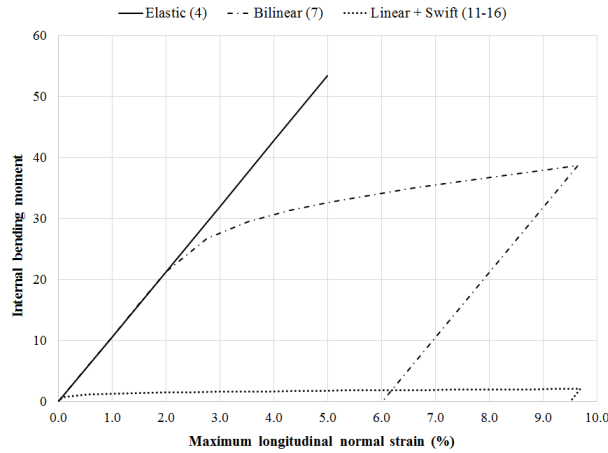
Figure 9: Comparison between the moment-strain functions for the cantilever of Figure 3.
The numbers in parenthesis denote the number of the corresponding equations.
The values of the strain and moment correspond to the values at the clamped edge.

4.2 First-mode buckling of cantilever

The second bending problem has been analyzed in order to verify the performance of the present method in predicting the post-buckling behavior of a cantilever under first-mode buckling. This problem has been widely studied and has important applications for engineering. When compared to the first beam problem analyzed in this paper, the only modification in Figure 3 is that the applied force is now horizontal and, thus, the bending moment along the curvilinear coordinate is $M(s) = Py = P\int_s \sin\theta \mathrm{d}s$. In this case, the corresponding boundary value problem and the system of IVPs are:

$$\frac{\mathrm{d}^2\theta}{\mathrm{d}s^2} = -\frac{P\sin\theta}{c}\left(\frac{\mathrm{d}M}{\mathrm{d}\varepsilon_{\max}}\right)^{-1}, \ \theta(L) = \frac{\mathrm{d}\theta}{\mathrm{d}s}(0) = 0 \tag{32}$$

$$\frac{\mathrm{d}f_1}{\mathrm{d}s} = f_2, \ f_1(0) = \theta_0 \tag{33}$$

$$\frac{\mathrm{d}f_2}{\mathrm{d}s} = -\frac{P\sin f_1}{c}\left(\frac{\mathrm{d}M}{\mathrm{d}\varepsilon_{\max}}\right)^{-1}, \ f_2(0) = 0 \tag{34}$$

As in the first example, the cantilever has been divided into 50 segments and, in the case of reaching the elastoplastic regime, the integration along the elastoplastic part is also performed with 50 segments. For the present beam problem, only the elastic and bilinear elastoplastic materials of Figure 3 have been considered.

Considering the elastic material coefficients of Figure 3, the critical load is:

$$P_{cr} = \frac{\pi^2 EI}{4L^2} = 13.1595 \ \text{or} \ \left(\frac{P}{EI}\right)_{cr} = \frac{\pi^2}{4L^2} = 0.6169 \tag{35}$$

According to Figure 10, the results of the present method regarding the linear-elastic material are in good agreement with Pai and Palazotto (1996), which employed the nonlinear multiple shooting method in order to solve equation (32). As the differences in Figure 10 are too small, the consideration of extensionality and shear effects, which leads to a more complex solution procedure, is not necessary. Along the pre-buckling stage, the displacements are null as the axial effects are neglected in the present formulation. As expected, the cantilever becomes unstable after the critical load (35), bending under the action of any eccentric axial force. One should remember that, even for an applied force larger than the critical load (35), if the first try for the free-end rotation θ_0 (see expression (33)) is very small (or close to zero), the cantilever will not bend, acting as a column under axial force. Thus, in order to trigger the buckling after the critical load, a sufficiently large value for the first θ_0 must be used. To illustrate this fact, for the larger applied force used in this example ($P/EI = 2.4674$), the influence of the first try for θ_0 on the cantilever behavior is provided in Table 4, in which one can see that the beam will not buckle if this first try is sufficiently small.
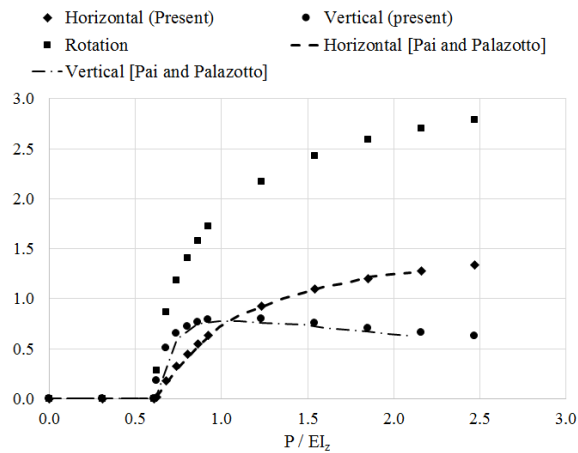
Figure 10: Free-end rotation and non-dimensional displacements for the cantilever under first-mode buckling composed of elastic material.

First try for θ_0	Solution for θ_0
0.100	0.000
0.500	0.000
1.000	0.000
1.500	0.000
2.000	2.788
2.500	2.788

Table 4: Solutions for some values of the first free-end rotation try.

In the context of elastoplastic post-buckling, only the bilinear material is used, and the final results are compared with the elastic case (see Figure 11). One can note that, as expected, the elastoplastic cantilever is more flexible than the elastic one, as the rigidity regarding the stress-strain relation decreases along the elastoplastic regime for the bilinear material (see the coefficients of Figure 3).
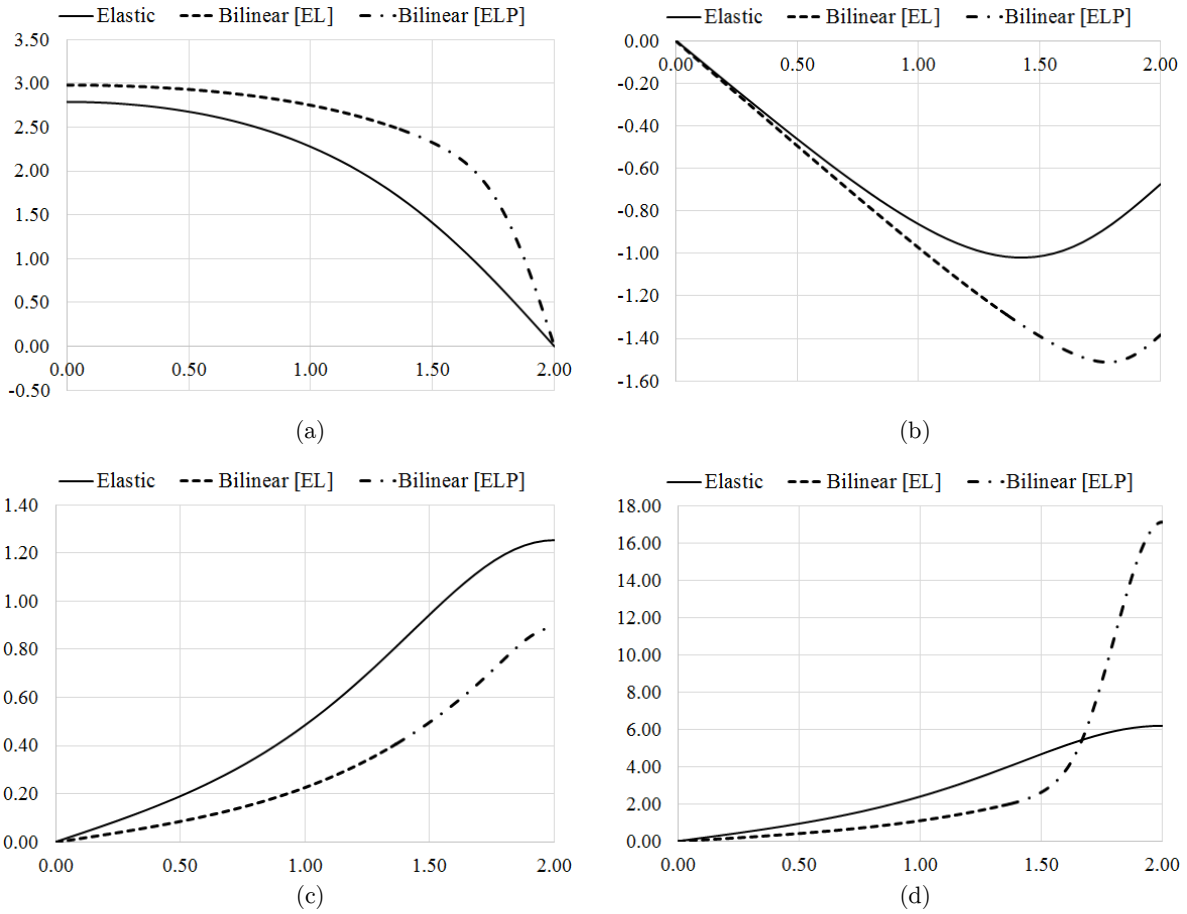
Figure 11: Comparison of results along the cantilever ($0.0 < s < 2.0$) under first-mode buckling at the last step ($P/EI = 2.4674$): (a) angle of rotation; (b) rectangular coordinate x; (c) rectangular coordinate y; (d) maximum cross-sectional normal strain (%). The symbols "[EL]" and "[ELP]" denote the elastic and elastoplastic regimes.
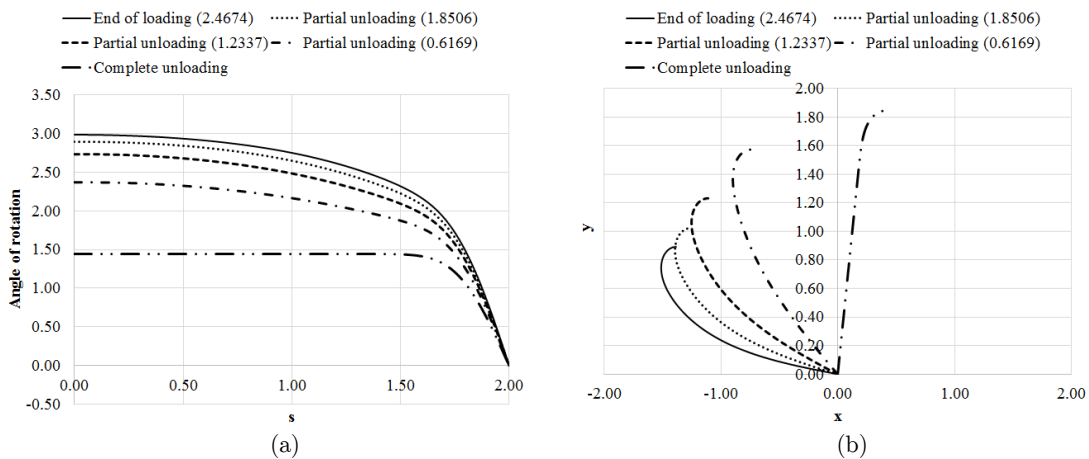
Figure 12: Numerical results along the complete and partial unloading phases for the cantilever under first-mode buckling composed of bilinear elastoplastic material: (a) angle of rotation; (b) rectangular coordinates. The number in parenthesis denotes the load factor P / EI .

Besides, the level of strain at the clamped edge reaches the value of 17,11%, which can be considered a moderate strain. Thus, further extensions to finite strain levels can be performed in future studies, because if the curvature becomes too large, due to Poisson effect the position of the neutral line is changed and, hence, the strain distribution of Figure 2 can no longer be employed. With respect to the unloading and reloading phases, some configurations regarding the angle of rotation and the rectangular coordinates along these phases are given in Figure 12. Comparing with Figure 8, the differences among the load levels in the beam behavior are much higher for the present example, and the elastic part also stays straight at the end of the unloading.

For the bilinear elastoplastic material, the unloading phase is addressed via a specific problem: the U-bending. The question to be answered numerically is: what is the value of the force that must be applied in order to make the cantilever becomes a U-shaped bar when the load is completely removed? Although theoretical, this problem has practical applications as in metal-forming processes, for instance. To solve such a problem, the value of the applied force is updated until the free-end rotation at the end of the complete unloading phase reaches the value of $\pi/2$ rad (or 90°). The convergence analysis, regarding the value of the applied force, is given in Table 5. After the two first tries, the one-dimensional secant method (see expression (28)) is employed to estimate the next values of the applied force. Finally, for the applied force solution, the angle of rotation and the maximum strain level at the end of the complete unloading are provided in Figure 13. Even after the complete unloading phase, the normal strain reaches a maximum value of 15%, which is a moderate level.

P/EI	θ_0
2.3438	1.4148
2.8125	1.5255
3.0041	1.5627
3.0462	1.5703
3.0488	1.5708
3.0489	1.5708

Table 5: Convergence analysis regarding the applied force for the U-bending problem.

(a)   (b)
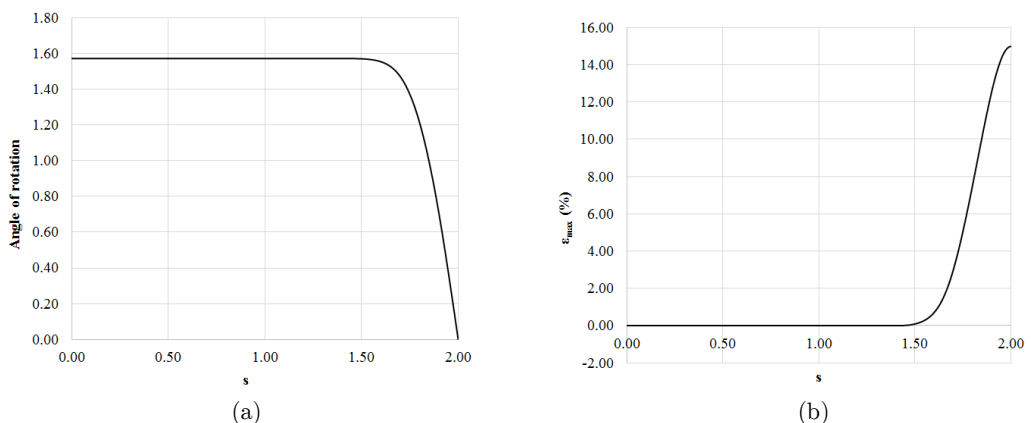
Figure 13: Final results for the U-bending problem (end of the complete unloading phase): (a) angle of rotation; (b) maximum normal strain at the clamped edge (%).

4.3 Buckling of a cantilever under a uniform distributed force

Another problem in which the present formulation can be evaluated is the buckling of a cantilever under a uniformly distributed horizontal load (see Figure 3). This bending problem is similar to the second example, and the only modifications are in equations (32) and (34):

$$\frac{\mathrm{d}^2\theta}{\mathrm{d}s^2} = -\frac{ws\sin\theta}{c}\left(\frac{\mathrm{d}M}{\mathrm{d}\varepsilon_{\max}}\right)^{-1}, \quad \theta(L) = \frac{\mathrm{d}\theta}{\mathrm{d}s}(0) = 0 \tag{36}$$

$$\frac{\mathrm{d}f_2}{\mathrm{d}s} = -\frac{ws\sin f_1}{c}\left(\frac{\mathrm{d}M}{\mathrm{d}\varepsilon_{\max}}\right)^{-1}, \quad f_2(0) = 0 \tag{37}$$

where w is the uniform load. Regarding the constitutive modeling, two materials are considered: linear-elastic with and without isotropic hardening. The elastic Young modulus adopted is $E = 210\,\mathrm{GPa}$. Thus, from linear theory and using the dimensions of Figure 3, the critical buckling load in elastic regime is:

$$\left(\frac{wL^3}{EI_z}\right)_{cr} = 7.837 \Rightarrow \left(\frac{w}{EI_z}\right)_{cr} = 0.9796 \Rightarrow w_{cr} = 20.8987 \tag{38}$$

According to Figure 14, the present elastic solution in terms of displacements is in agreement with the critical load (38) and also with Holden (1972). Besides displacements, the free-end rotation for each load level used is also given in Figure 14.
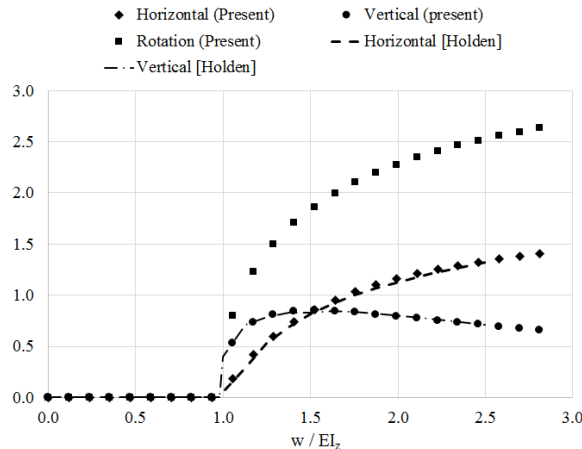
Figure 14: Free-end rotation and non-dimensional displacements for the linear-elastic cantilever under a uniformly distributed buckling force.

In the context of elastoplasticity, this problem has also been numerically analyzed by Lewis et al. (1987), which developed a formulation similar to the present study: definition of the differential equation regarding the angle of rotation; axial and shear effects neglected; partially yielded rectangular cross section; and solution by means of variational principles. However, it is not clear if the

material adopted by those authors is perfectly elastoplastic or bilinear elastoplastic. Thus, comparison of their results with the present ones is not possible. For the present example, in order to evaluate the influence of the isotropic hardening model on the beam behavior, four values for the Swift coefficient n (see equation 10) have been adopted (see Table 6). In all the four cases, after the beam buckles ($w = w_{cr}$), the uniform load reaches the value of 40.0 ($w/w_{cr} = 1.914$), returns to zero, is increased to 60.0 ($w/w_{cr} = 2.871$) and then returns to zero again.

Regarding the numerical results for the second material, the four cases analyzed provide similar behaviors and, as expected, increasing the Swift coefficient n leads to more flexibility (see Figures 15-17). From Table 6, one can note that, keeping the coefficients K and ε_0 constant, an increase in the value of n provides lower values for the yield stress and strain limits, which provides more flexibility for the cantilever in elastoplastic regime. Another point to be highlighted is that, along the first unloading and reloading phases, the behavior of the beam is purely elastic. Finally, as in the second example, the accordance of results with the critical load (38) means that the beam buckles in elastic regime. The only caveat to be taken into account is the levels of strain after the beam buckles, which can be considered moderate (see Figures 16 and 17). As in Figure 13, the strain values of Figure 17 correspond to the maximum plastic (or permanent) strain at the cross sections.

K (GPa)	ε_0	n	σ_Y (GPa)	ε_Y (%)
		0.05	7.94	3.78
10	0.01	0.10	6.31	3.00
		0.15	5.01	2.39
		0.20	3.98	1.90

Table 6: Swift coefficients, yield stress and yield strain for the third example.

5 CONCLUSIONS

In this paper, a numerical formulation for analysis of highly deformable elastoplastic thin beams is presented. The following concepts are employed in the present methodology: Euler-Bernoulli bending; nonlinear second-order differential equation regarding the angle of rotation; moment-curvature relationship based on the uniaxial stress-strain elastoplastic model; fourth-order Runge-Kutta integration procedure; and one-parameter nonlinear shooting method. The formulation is applied to three flexible and thin cantilevers composed of elastoplastic material: free-end shear force; first-mode buckling; and buckling under uniformly distributed force. For these three examples, many numerical solutions regarding the structural behavior are provided. The results in the context of elastic regime are in agreement with the corresponding reference data. Although the numerical examples are quite simple, the basic formulation can be applied to problems involving flexible elastoplastic beams with other boundary conditions, cross-sections and constitutive models. The procedure is to define the relation of the bending moment with the maximum longitudinal strain and with the curvilinear coordinate.

One of the contributions of this paper is the development of the explicit relations between the internal bending moment and the maximum longitudinal strain for the bilinear elastoplastic material and the linear-elastic material with Swift isotropic hardening. Besides, the numerical results are
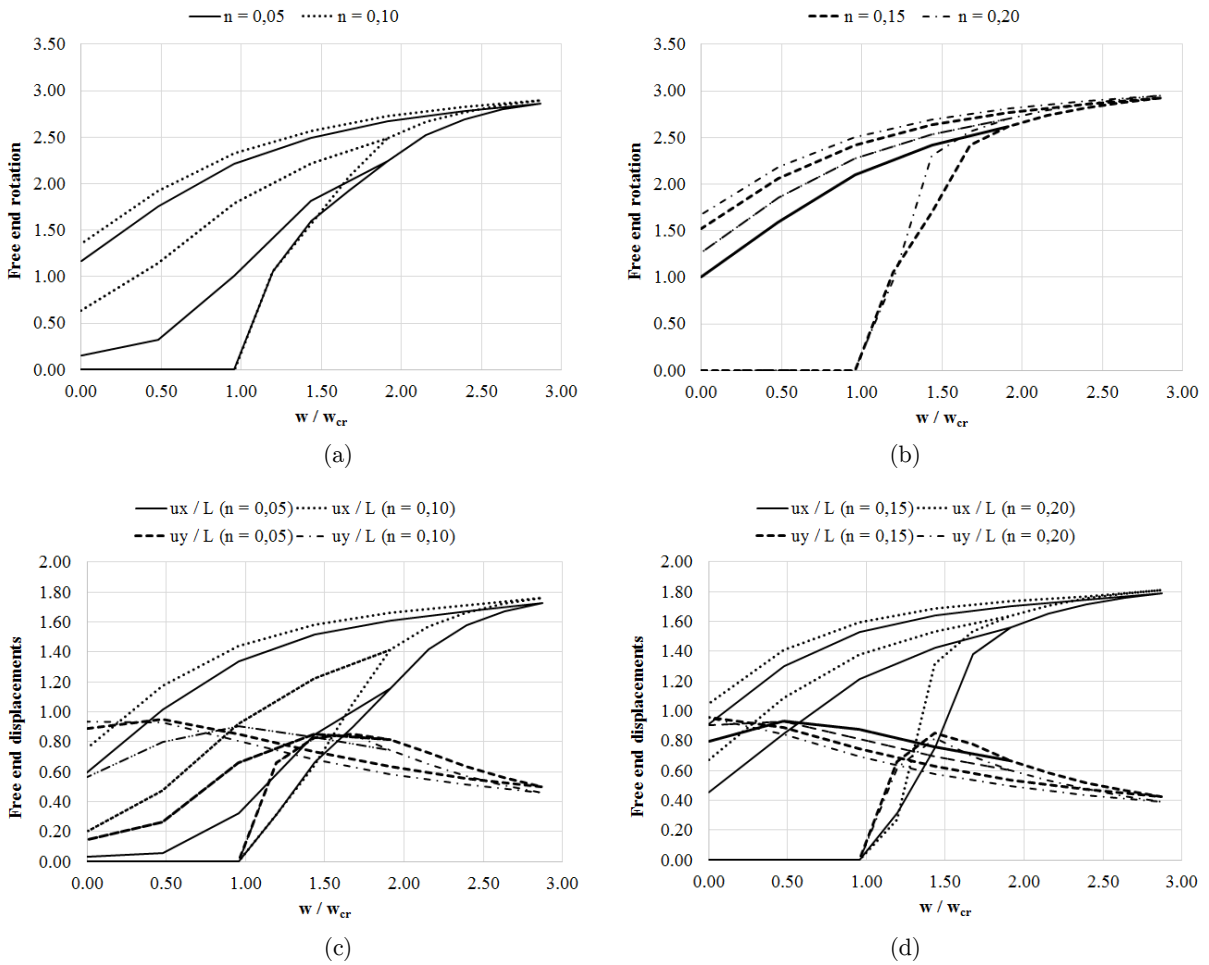
Figure 15: Free-end non-dimensional displacements and angle of rotation for the elastoplastic cantilever under a uniformly distributed load. The symbol "w_{cr}" denotes the critical load (38).
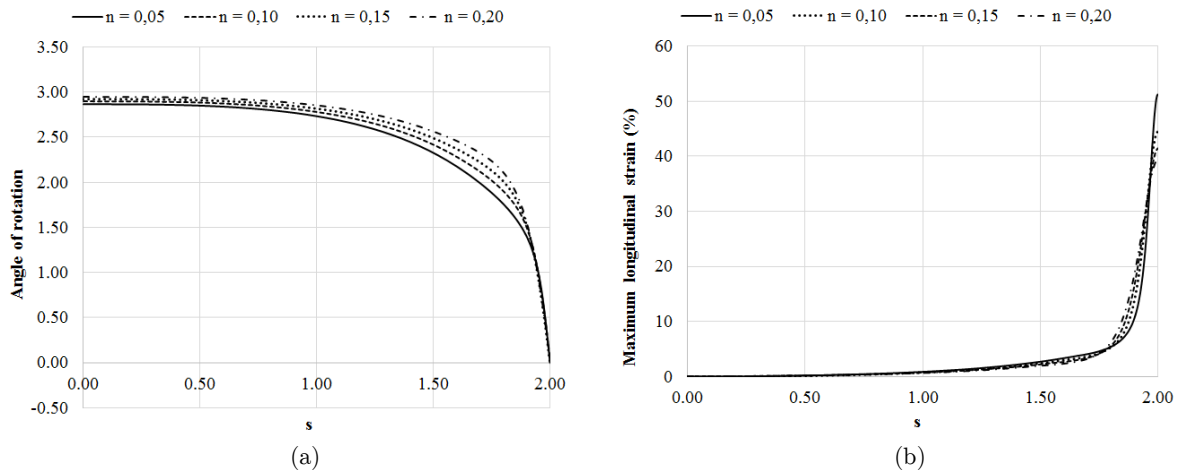
Figure 16: Results for the maximum load level ($w = 60.0$) along the elastoplastic cantilever under a uniformly distributed load.
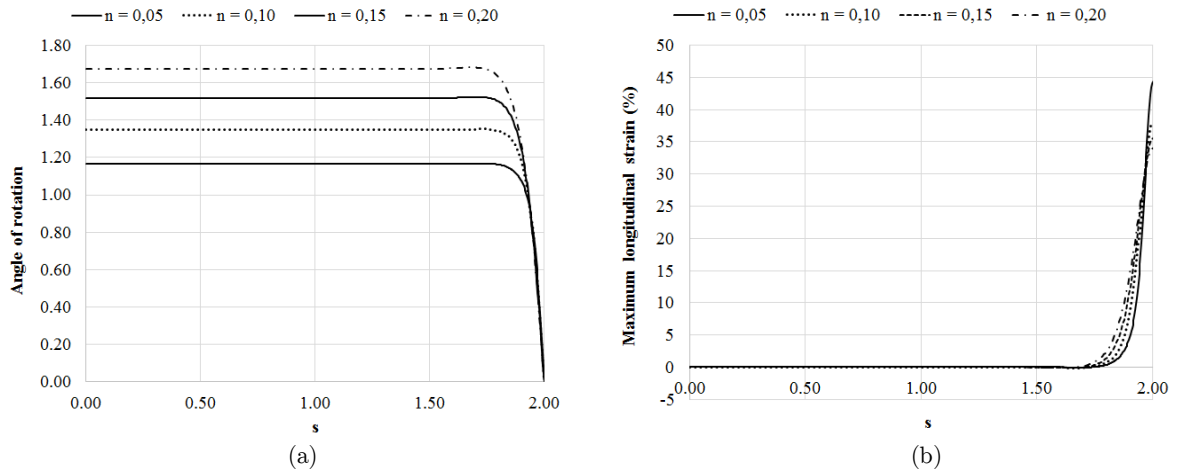
Figure 17: Results for the last stage (complete unloading after the maximum load) along the elastoplastic cantilever under a uniformly distributed load.

also provided in terms of the angle of rotation and the maximum strain along the length of the beam, not only the relation between the applied force versus free-end displacements and rotation. These results can be compared with future studies regarding the mechanical behavior along the beam. Another feature of the present study is the analysis of highly deformable elastoplastic beams along the unloading and reloading phases, which is a topic rarely addressed in the scientific literature. As expected, after the load is completely removed, the elastic portion of the beam stays straight and the elastoplastic part remains curved. In respect to buckling problems, the present formulation can be used to predict the instability, and numerical solutions for post-buckling behavior are given. Regarding the constitutive modeling, as the levels of longitudinal normal strain reaches moderate values, future extensions to nonlinear finite-strain elastoplastic models can be performed. It is worth saying that the application of the present technique to hyper-static beam problems can be made in future studies. Finally, due to the simplicity in solving post-buckling problems, the present formulation can be employed, for instance, in nonlinear analysis of truss-like structures composed of elastoplastic compressed members.

Acknowledgements

References

Bisshopp, K.E., Drucker, D.C., (1945). Large deflection of cantilever beams. Q. Appl. Math 3: 272-275.

Carrillo, E.S., (2009). Semi-exact solutions for large deflections of cantilever beams of non-linear elastic behavior. International Journal of Non-linear Mechanics 44: 253-256.

Chan, S.L., Kitipornchai, S., Al-Bermani, F.G.A., (1991). Elasto-plastic analysis of box-beam-columns including local buckling effects. Journal of Structural Engineering 117: 1946-1962.

Chen, L., (2010). An integral approach for large deflection cantilever beams. International Journal of Non-linear Mechanics 45: 301-305.

Cimetière, A., Léger, A., (1996). Some problems about elastic-plastic post-buckling. International Journal of Solids and Structures 33: 1519-1533.

Durban, D., Zuckerman, Z., (1999). Elastoplastic buckling of rectangular plates in biaxial compression/tension. International Journal of Mechanical Sciences 41: 751-765.

Grognec, P.L., Le van, A., (2011). On the plastic bifurcation and post-bifurcation of axially compressed beams. International Journal of Non-linear Mechanics 46: 693-702.

Holden, J.T., (1972). On The finite deflections of thin beams. International Journal of Solids and Structures 8: 1051-1055.

Hutchinson, J.W., (1972). On the postbuckling behavior of imperfection-sensitive structures in the plastic range, Journal of Applied Mechanics 71: 155-162.

Jenkins, J.A., Seitz, T.B., Przemieniecki, J.S., (1966). Large deflection of diamond-shaped frames. International Journal of Solids and Structures 2: 591-603.

Kounadis, A.N., Mallis, J.G., (1987). Elastica type buckling analysis of bars from non-linearly elastic material. International Journal of Non-linear Mechanics 22: 99-107.

Lee, K., (2002). Large deflections of cantilever beams of non-linear elastic material under a combined loading. International Journal of Non-linear Mechanics 37: 439-443.

Léger, A., Potier-Ferry, M., (1993). Elastic-plastic post-buckling from a heterogeneous state. Journal of the Mechanics and Physics of Solids 41: 783-807.

Lewis, G., Monasa, F., (1981). Large deflections of cantilever beams of nonlinear materials. Computers Structures 14: 357-360.

Lewis, G., Mazilu, P., Monasa, F., (1987). A variational approach for the deflections and stability behavior of post-buckled elastic-plastic slender struts. International Journal of Non-linear Mechanics 22: 373-385.

Mattiasson, K., (1981). Numerical results from large deflection beam and frame problems analyzed by means of elliptic integrals. Short Communications: 145-153.

Monasa, F., Lewis, G., (1983). Large deflections of point loaded cantilevers with nonlinear behavior. Journal of Applied Mathematics and Physics. 34: 124-130.

Pai, P.F., Palazotto, A.N., (1996). Large-deformation analysis of flexible beams. International Journal of Solids and Structures 33: 1335-1353.

Rao, B.N., Rao, G.V., (1989). Large deflections of a cantilever beam subjected to a rotational distributed loading. ForschungimIngenieurwesen Bd. 55: 116-120.

Sinclair, G.B., (1979). The non-linear bending of a cantilever beam with shear and longitudinal deformations. International Journal of Non-linear Mechanics 14: 111-122.

Swift, H., (1947). Length changes in metals under torsional overstrain. Eng. 163: 253-257.

Tari, H., (2013). On the parametric large deflection study of Euler-Bernoulli cantilever beams subjected to combined tip point loading. International Journal of Non-linear Mechanics 49: 90-99.